Electronic Supplementary Material (ESI) for RSC Advances.

Supporting Information:
Dispersion Forces Drive Water Oxidation in Molecular Ruthenium Catalysts

Mikael P. Johansson[1,2,3,a,*], Lukas Niederegger[2,a], Markus Rauhalahti[1], Corinna R. Hess[2,*] and Ville R. I. Kaila[2,4,*]

[1] Department of Chemistry, University of Helsinki, P.O. Box 55, FI-00014 Helsinki, Finland.
[2] Department Chemie, Technical University of Munich (TUM), Lichtenbergstraße 4, Garching D-85747, Germany.
[3] Helsinki Institute of Sustainability Science, HELSUS, FI-00014 Helsinki, Finland.
[4] Department of Biochemistry and Biophysics, Stockholm University, Stockholm, Sweden.
[a] Contributed equally to this work.
[*] E-mail: mikael.johansson@helsinki.fi; corinna.hess@tum.de; ville.kaila@dbb.su.se

Table of Contents

METHODOLOGY

Quantum Chemical Calculations

The geometries of the studied ruthenium catalyst models, ruthenium-2,2′-bipyridine-6,6′-dicarboxylic-acid-dibenz[g]isoquinoline, Ru-BdaBenz$_2$ (**3**), ruthenium-2,2′-bipyridine-6,6′-dicarboxylic-acid-di isoquinoline, Ru-BdaIsoq$_2$ (**2**), and ruthenium-2,2′-bipyridine-6,6′-dicarboxylic-acid-di-4-picoline, Ru-BdaPic$_2$ (**1**) were optimized in Ru^{IV} and Ru^{V} states, with oxo- and dioxygen ligands, at density functional theory (DFT) level, using the TPSSh-D3(BJ) hybrid functional corrected for dispersion interactions[1–4], in combination with the def2-TZVPD basis set for the Ru=O unit, and def2-SVP for the other atoms[5,6]. Final electronic energies were computed using the def2-QZVPP basis sets, with added diffuse functions (def2-QZVPPD) on the Ru=O unit. Solvation effects were treated using the conductor-like screening model (COSMO)[7] with a dielectric constant of 78, mimicking the dielectric response of an aqueous environment. The dimeric models, comprising 108-144 atoms, are shown in **Figure 1** (main text). Reaction paths for the O-O bond formation process were studied using multi-dimensional reaction path optimization approach[8], related to the zero-temperature string method[9]. Based on the optimized reaction paths, transition state optimizations for the central models were performed. For comparison, the electronic energies of selected points along the reaction path were computed with the random phase approximation (RPA) using TPSSh orbitals [10-13]. The RPA correlation energy was extrapolated towards the complete basis set (CBS) limit using the two-point formula by Halkier *et al*.[14] in connection with the def2-TZVPP(D) and def2-QZVPP(D) basis sets, with diffuse functions on the heavy atoms of the axial ligands and the Ru=O unit, in order to properly account for dispersion effects. Entropic and enthalpic effects were evaluated using the harmonic oscillator approximation, with possible low-frequency modes below 50 cm^{-1} set to 50 cm^{-1}. The full molecular Hessian was computed using numerical second derivatives. Non-covalent interaction (NCI) analyses were performed with NCIplot version[15,16] and visualized with VMD[17]. Energy decomposition analyses were performed within the Su-Li scheme[18]. All quantum chemical calculations were performed using TURBOMOLE[19,20].

Synthesis of Ru-BdaBenz$_2$ (3)

Ru(DMSO)$_4$Cl$_2$ (200.0 mg, 0.4 mmol), 2,2’-bipyridine-6,6’-dicarboxylic acid (H_2bda) (100.8 mg, 0.4 mmol) and NEt_3 (0.84 mL, 6 mmol) were mixed in 60 mL of methanol. The solution was sparged with Ar for 15 min and stirred at 70° C for 2 h. Upon heating the solution became dark red. Benz[g]isoquinoline (740 mg, 4 mmol) was added and the reaction was stirred overnight. The solvent was removed and the crude product was purified by column chromatography on silica using a DCM:MeOH gradient (100:1, 25:1, 25:2). The red brown solid obtained after solvent removal was washed with water and ether. Afterwards, the dark red solid was dissolved in DCM, filtered and the solvent was removed. After recrystallization from MeOH, 50 mg of **3** (0.07 mmol, 17%) were obtained as a dark red solid. Single crystals suitable for X-ray diffraction were obtained by slow diffusion of pentane into a solution of **3** in DCM.
R_f value (25:1) = 0.13
UV/Vis λ_{max} (DCM)/nm 493, 402, 381, 351, 331 and 301 (ε /M^{-1} x 10^3 cm^{-1} 11.1, 9.0, 9.5, 11.5, 8.4, 22.9);
^{1}H-NMR (400 MHz, CD_2Cl_2): δ [ppm] 8.81 (s, 2H, H_4, H_4'), 8.75 (d, J = 7.95 Hz, 2H, H_3, H_3'), 8.57 (s, 2H, H5, H_5'), 8.45 (s, 2H, H_{10}, H_{10}'), 8.08 (m, 6H, H_1, H_1', H_6, H_6', H_9,H_9'), 7.98 (t, J = 7.86 Hz, 2H, H_2, H_2'), 7.73 (d, J = 6.90 Hz, 2H, H_{12}, H_{12}'), 7.63 (m, 6H, H_7, H_7', H_8, H_8', H_{11}, H_{11}')
LRMS (ESI) m/z = 703.12 $[M+H]^+$

Experimental conditions

Chemicals were purchased from Sigma Aldrich and used as received unless otherwise noted. 2,2'-Bipyridine-6,6'-dicarboxylic acid was purchased from TCI. Ferrocene was purified via sublimation and tetrabutylammonium hexafluorophosphate ($TBAPF_6$) was recrystallized from ethanol three times. The aqueous pH = 1 solution of trifluoromethansulfonic (triflic) acid was prepared by diluting 10 g of triflic acid (5.88 mL) with 662 mL of deionised water. Reactions requiring inert atmosphere were performed using standard Schlenk techniques and dry, de-oxygenated solvents. Solvents were dried by passage over activated alumina columns from MBraun and stored over 3 Å or 4 Å molecular sieves. $Ru(DMSO)_4Cl_2$[21], $Ru(bda)(isoquinoline)_2$[22] and benz[g]isoquinoline[23] were prepared according to literature procedure with the following modifications: 1-(Phenoxycarbonyl)-4-(benzyl)-1,4-dihydropyridine-3-carboxaldehyde was purified via filtration over silica using ether:hexane = 2:1. The resultant yellow oil was stirred with hexane and the product was filtered off as a white solid. The crude mixture of 4-benzylpyridine-3-carboxaldehyde was purified via column chromatography using ether as the eluent (R_f = 0.36). Purity of literature-known compounds was verified by NMR.

Physical measurements

Nuclear magnetic resonance (NMR) measurements were performed with a Bruker Avance Ultrashield (400 MHz ^1H). Electronic spectra were measured on an Agilent Cary 60 UV-visible spectrophotometer. ESI mass spectra were recorded on a Waters TQD instrument.

Crystallography

The crystallographic data was collected on a X-ray single crystal diffractometer, equipped with a CCD detector (Bruker APEX II, κ-CCD), a rotating anode (Bruker AXS, FR591) with Mo K_α radiation (λ = 0.71073 Å) and a MONTEL mirror optic by using the $APEX_3$ software package[24]. The crystal was picked from perfluorinated ether and fixed on top of a Mitegen® microsampler and transferred to the diffractometer. The measurement was carried out under a constant stream of cold nitrogen. A matrix scan was used to determine the initial unit cell parameters. SAINT[25] as implemented in the APEX3 suite was used to merge and correct the reflections for Lorenz and polarization effects, scan speed, and back ground. Absorption corrections containing odd and even ordered spherical harmonics were performed using SADABS[26]. Space group assignments were established using systematic absences, E statistics, and successful refinement of the structures. Structures were solved using the intrinsic phasing method (SHELXT), which also supported the correct assignment of the space groups, and were refined against all data using SHELXLE in conjunction with SHELXL-2014 [27-29]. Hydrogen atoms were calculated to the ideal position and refined employing a riding model with isotropic thermal parameters. Non-hydrogen atoms were refined with anisotropic displacement parameters. The images of the crystal structure were generated using Mercury[30]. Using Platon[31] Squeeze 284 electrons in a solvent accessible void of 823 $Å^3$ were determined corresponding to seven pentane molecules (294 electrons) for **3** and 109 electrons in a solvent accessible void of 399 $Å^3$ were determined for **2** corresponding to 2.5 pentane molecules (105 electrons).

*Refinement of **3**:*

Protons of the water molecule were located according to the residual electron density (Figure below) and the position of H43 was not refined.

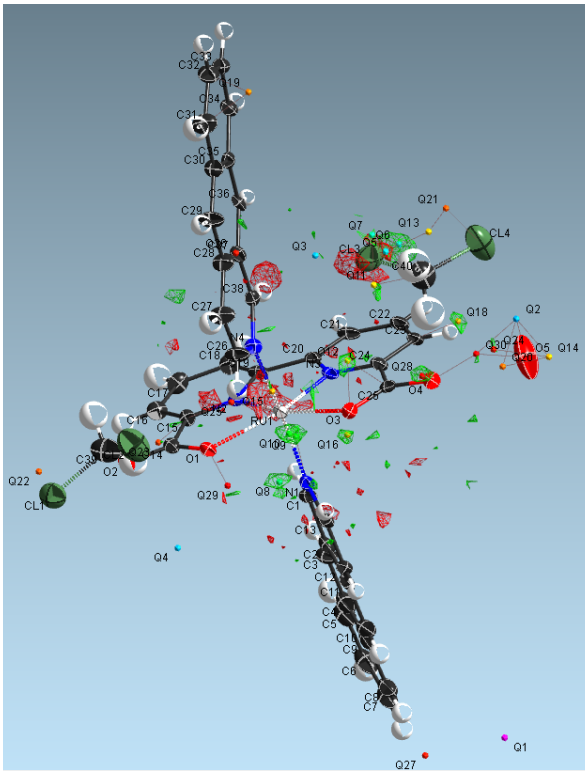

Absorption spectroscopy

pH dependence of the absorption spectra

A stock solution of **3** (solution A) was prepared by dissolving a sample of the complex in 3 mL TFE (such that [**3**] = 1.4 mM), and the solution was stirred for 20 min. A 0.1 mL aliquot was removed from solution A and diluted to 3 mL with TFE, and the absorption spectrum was recorded (**Figure S7**, black trace). Afterwards, 1.5 mL of a pH 1 solution were added to the stock solution (such that TFE/pH 1_{aq} = 2:1 = solution B), to mimic the catalytic conditions. After 4 h, a 0.1 mL aliquot was taken from solution B and diluted to 2 mL ([**3**] = 71 µM; Figure S8, red trace). Finally, 18 mg NaOH (3 eq. relative to the pH 1_{aq} solution) were added to solution B (solution C, final pH of the solution = 12). Solution C was stirred for 1 h, a sample was prepared for the absorption measurement as described above, and the spectrum recorded (**Figure S8**, blue trace). Catalyst **3** shows pH sensitive spectral changes (**Figure S7**) that can be attributed to changes in the coordination mode of the Bda ligand, as previously observed for **2** [33].

Electrochemistry experiments

Electrochemical measurements were carried out with an EmStat3+ potentiostat or a BioLogic SP-200 using glassy carbon (diameter = 3 mm) as working and counter electrodes, and either Ag/AgCl or $Ag/AgNO_3$ separated by a vycor frit as the reference electrode. A 5-neck flask was used: one inlet was used to flush the cell with argon, one inlet was used for the addition of the samples, and the remaining inlets were fitted with the counter, working and reference electrodes. All potentials are given vs NHE. For referencing, ferrocene was used as an internal standard and the potentials were adjusted to the NHE scale ($Fc^{+/0}$ = 400 mV vs. NHE). All cyclic voltammograms (CVs) were measured with a scan rate of 10 mV s^{-1}, unless otherwise noted. Differential Pulse Voltammetry (DPV) was measured with a pulse height of 50 mV, a pulse width of 2.5 s and step height of 4 mV, a step time of 5 s and a sampling time of 500 ms. For measurements in pure trifluoroethanol (TFE), tetrabutylammonium hexafluorophosphate ($TBAPF_6$; 0.1 M) was used as the electrolyte.

CV measurements under catalytic conditions

Due to the low solubility of **3** in aqueous solutions, electrochemical measurements under catalytic conditions were carried out in a 2:1, TFE/pH 1_{aq} mixture, instead of the 1:2, TFE/pH 1_{aq} solution previously used for electrocatalytic studies with **2**[22]. For measurements under catalytic conditions ca. 3.0 mg of **3** or **2** were dissolved in 6 mL of deoxygenated TFE, stirred for 5 min under Ar atmosphere and 3 mL of deoxygenated pH 1 solution were added. After stirring for an additional 10 min, the solution was transferred into the CV cell, under Ar. A rinse test experiment carried out after the electrocatalytic measurements confirmed that no complex is adsorbed on the electrode.

Comparison of different catalysts

The low solubility of **3**, and the proximity of the $Ru^{V/IV}$ couple to the catalytic onset potential causes difficulties in applying an accurate Foot of the Wave Analysis (FOWA). However, the relative activities of **2** and **3** can be estimated using the following equation[32]:

$$\frac{i_{cat,anodic}}{i_{p,anodic}} = \frac{1}{0.446}\sqrt{\frac{RT}{nFv}k_{obs}} \quad (1)$$

Here, i_{cat} refers to the maximum catalytic current, and $i_{p,\,anodic}$ refers to the current obtained for the $Ru^{V/IV}$ couple. The ratio of the rate constants, k_{obs}, for Ru-Benz and Ru-Iso, can therefore, be approximated using,

$$\frac{\left[\frac{i_{cat,anodic}}{i_{p,anodic}}\right]^2_{Ru-Benz}}{\left[\frac{i_{cat,anodic}}{i_{p,anodic}}\right]^2_{Ru-Iso}} = \frac{[k_{obs}]_{Ru-Benz}}{[k_{obs}]_{Ru-Iso}} \quad (2)$$

Figure S13 shows the CV of **2** and **3** in 2:1, TFE/pH 1_{aq} at a scan rate of 10 mV s^{-1}; the corresponding potential for $i_{p,anodic}$ and $i_{cat,anodic}$ are indicated by the vertical lines; the values obtained for three different measurements of each complex are listed in **Table S5**.

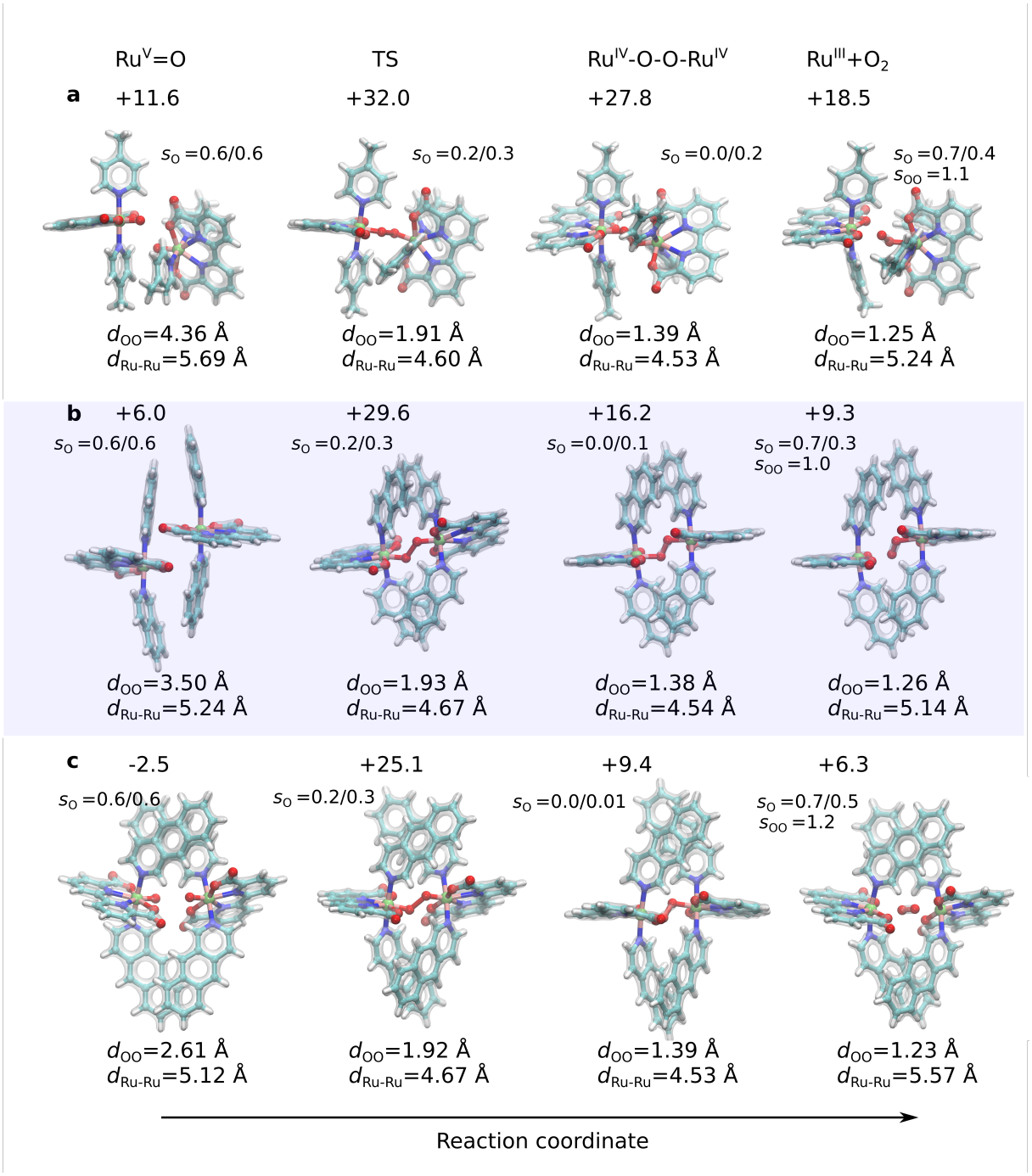

Figure S1. Structures along the optimized reaction pathway for catalyst a) **1**, b) **2**, and c) **3**. All structures are optimized in the open-shell triplet states.

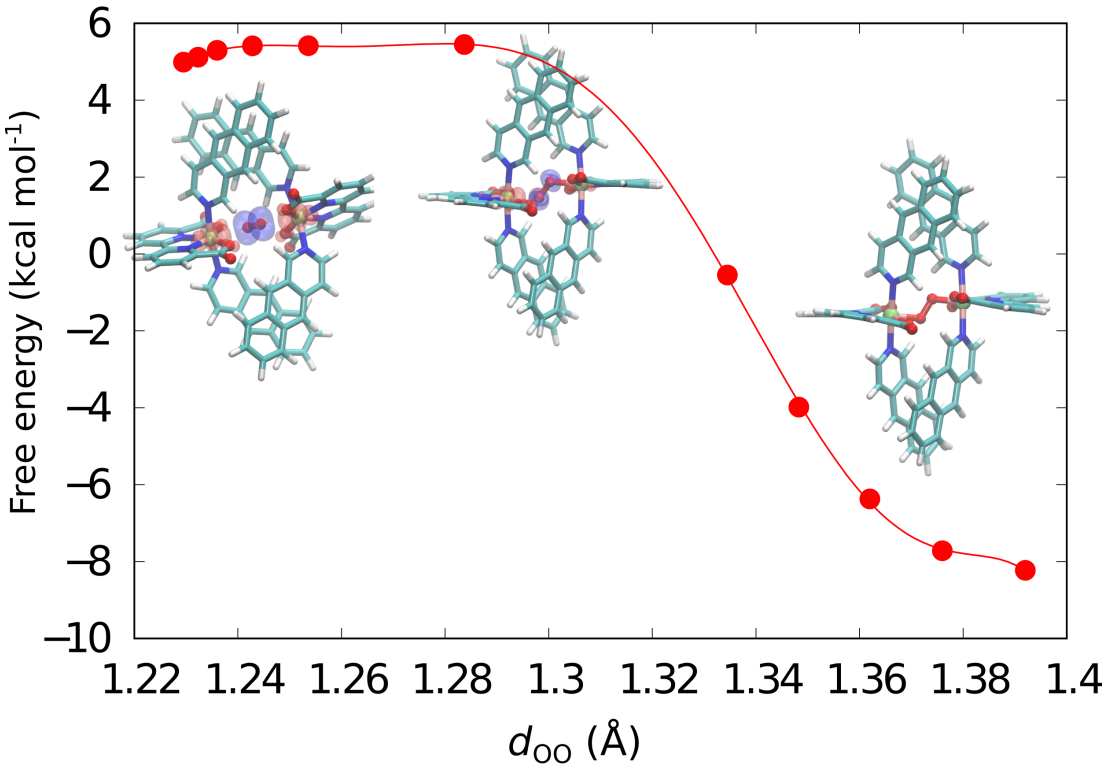

Figure S2. Close-up of the reaction coordinate of **3**, where the closed-shell singlet peroxy state (*d*oo≈1.4 Å) is transformed into the open-shell superoxide state preceding O_2 release (*d*oo≈1.2 Å). α (β) spin density is shown at ±0.005 isosurface threshold in blue (red).

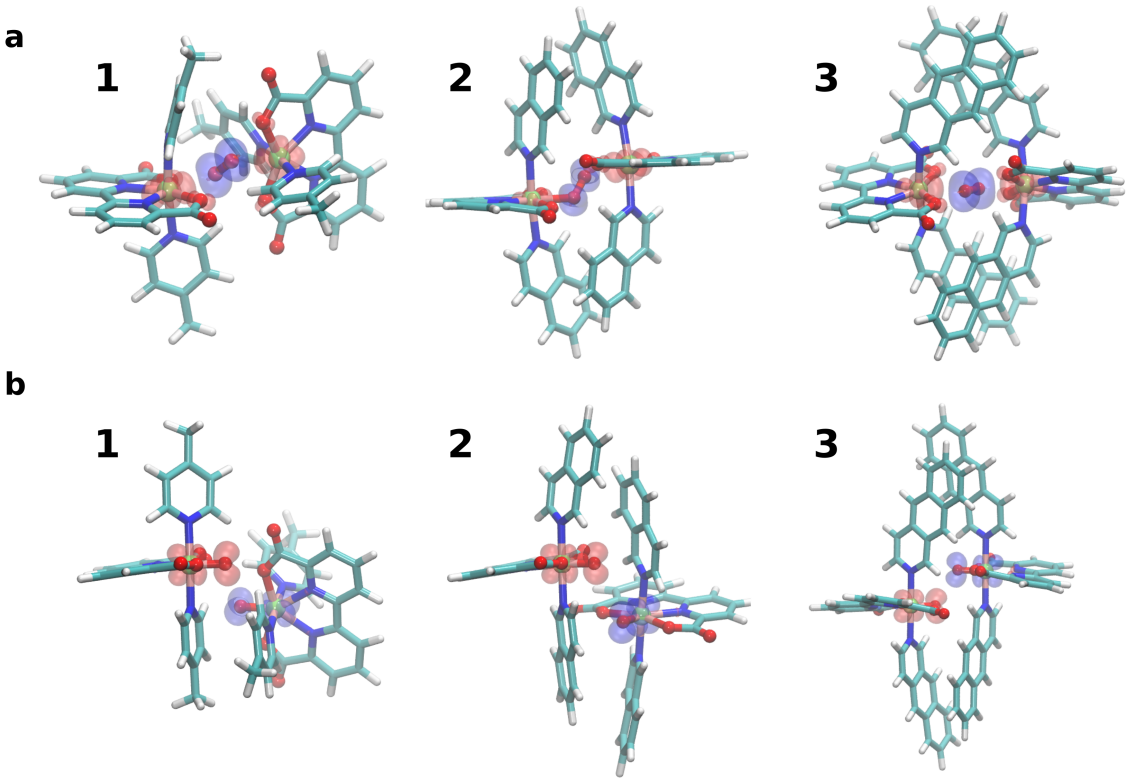

Figure S3. Spin density distributions for catalyst **1**, **2**, and **3** in a) the Ru-O_2 state and b) in the dimeric state. α (β) spin density is shown at ±0.005 isosurface threshold in blue (red).

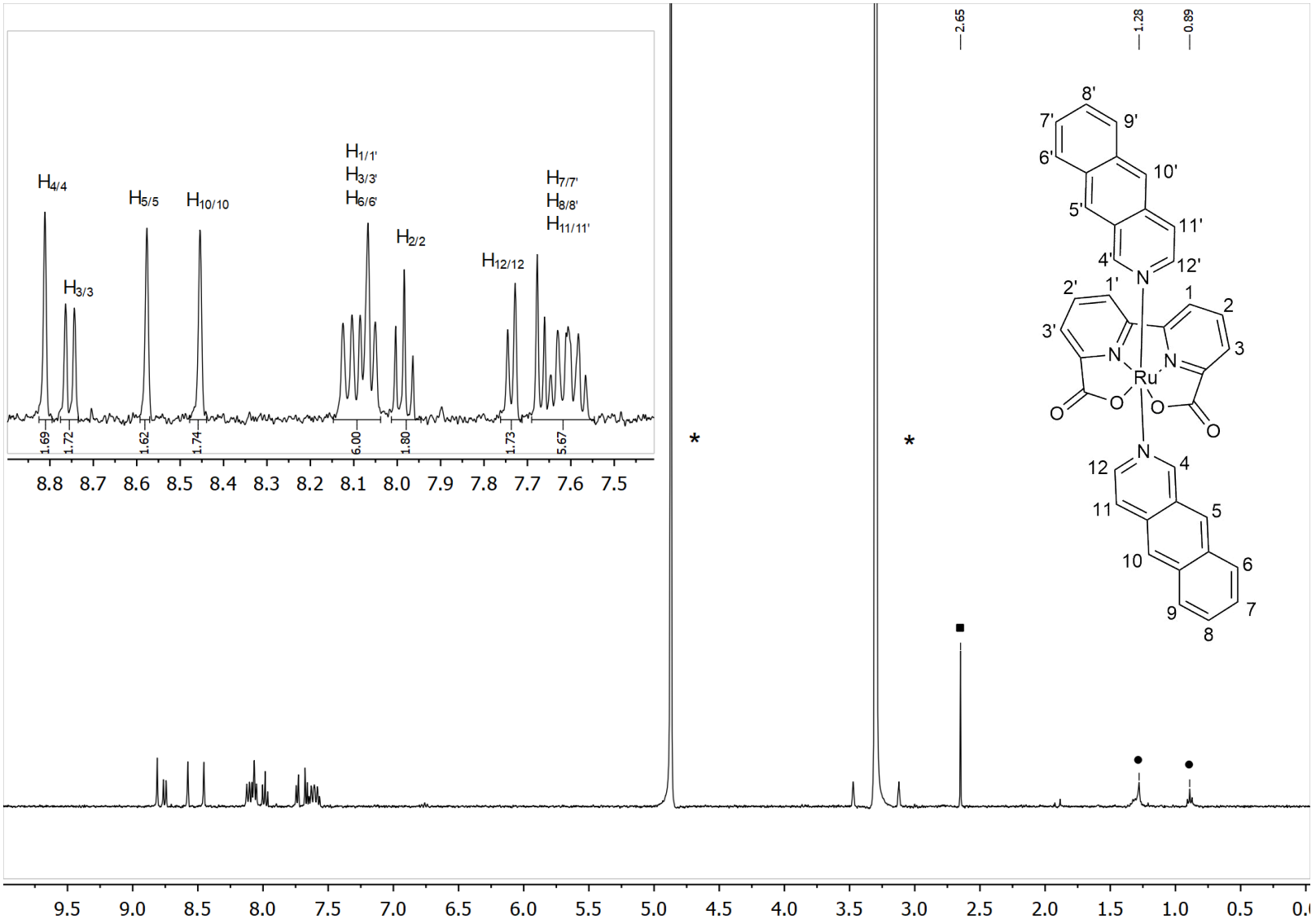

Figure S4. ^{1}H-NMR (400 MHz, CD_3OD) of **3**; * = *residual solvent peak and water,* ■ = *dmso,* ● = *grease.*

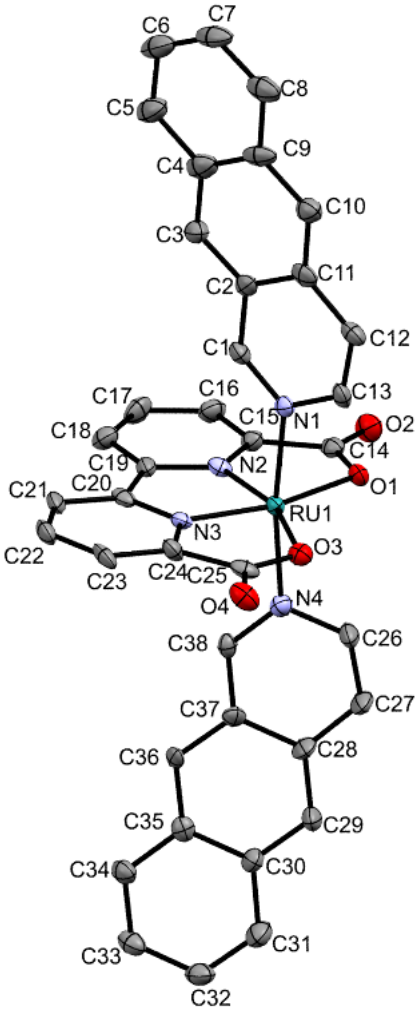

Figure S5. Molecular structure of **3** (50% probability ellipsoids). Hydrogen atoms and solvent molecules omitted for clarity.

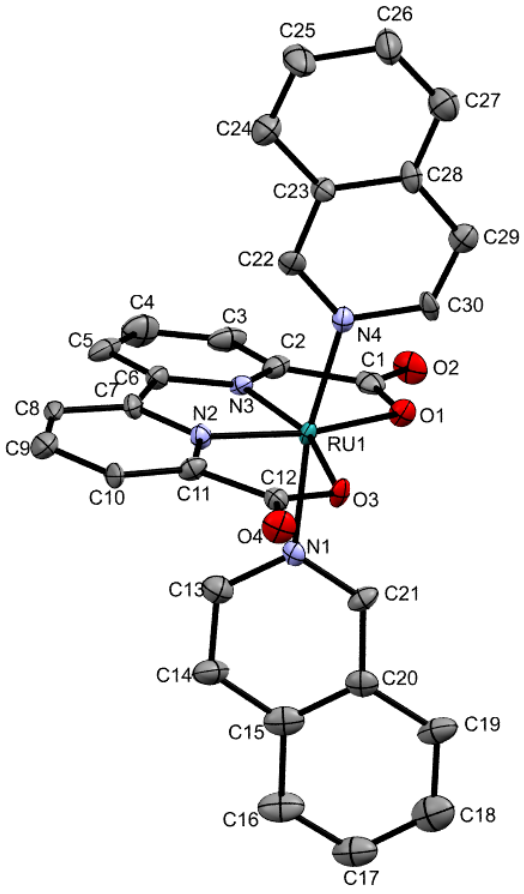

Figure S6. Molecular structure of **2** (50% probability ellipsoids). Hydrogen atoms and solvent molecules omitted for clarity.

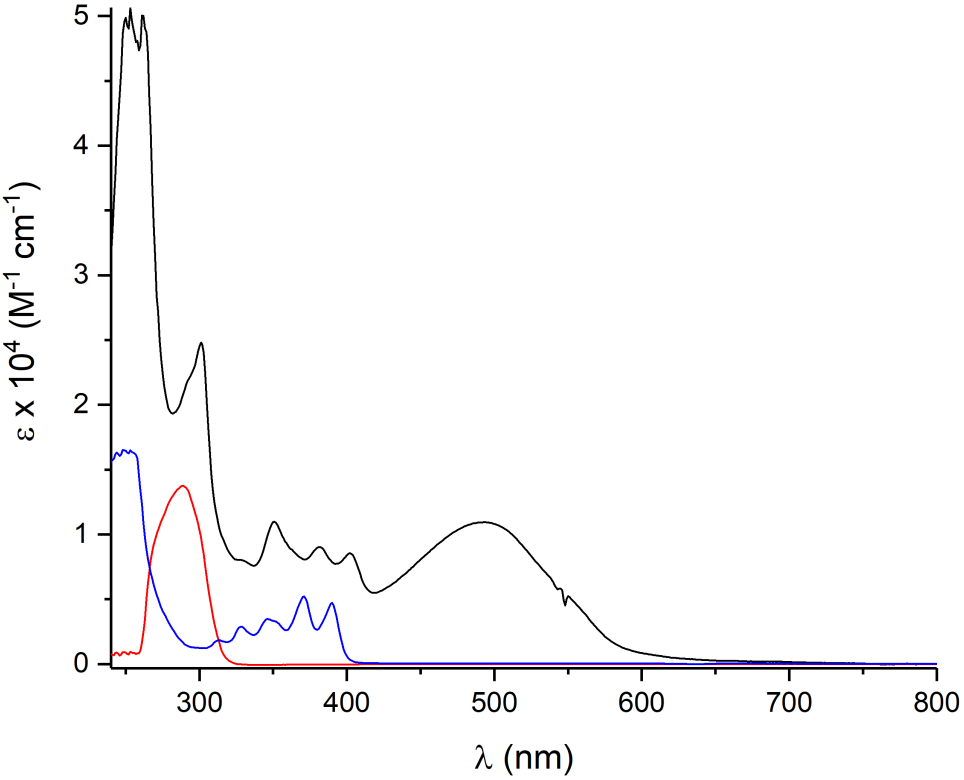

Figure S7. Absorption spectra of **3** (black), bda (red) and benz[g]isoquinoline (blue) in DCM. NEt_3 (15 %) was added for the bda measurement to enhance the solubility of this compound in DCM.

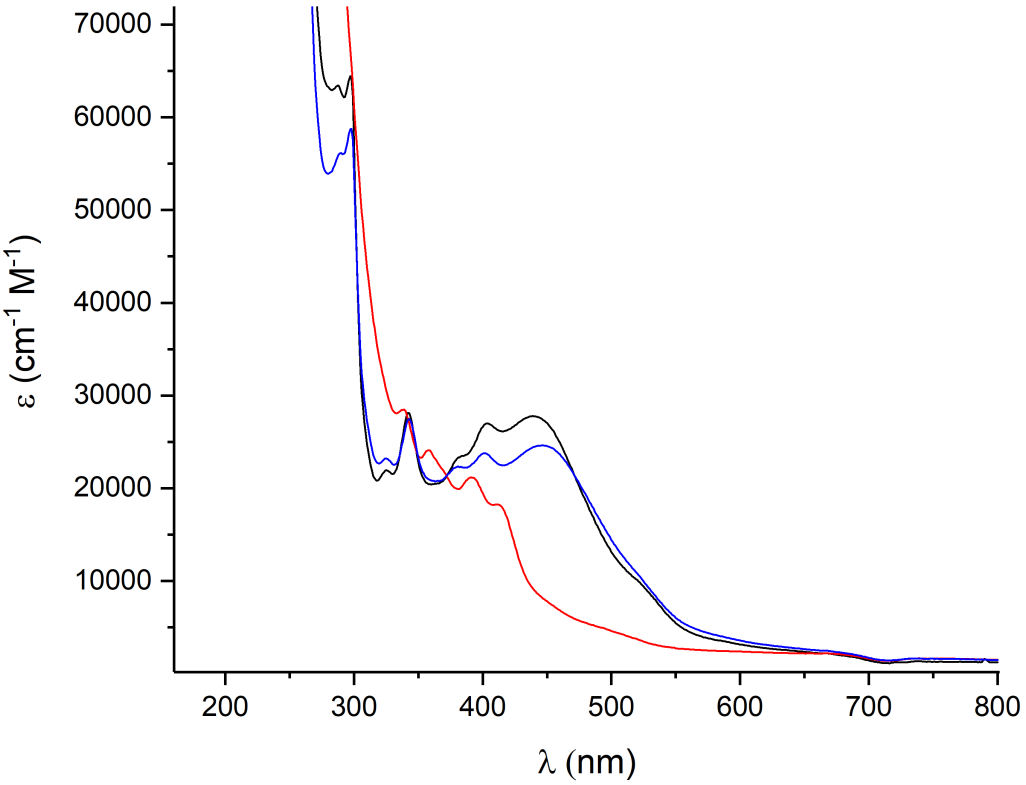

Figure S8. Absorption spectra of **3** in TFE only (black), after addition of the pH 1_{aq} solution (red), and after neutralization with NaOH (blue).

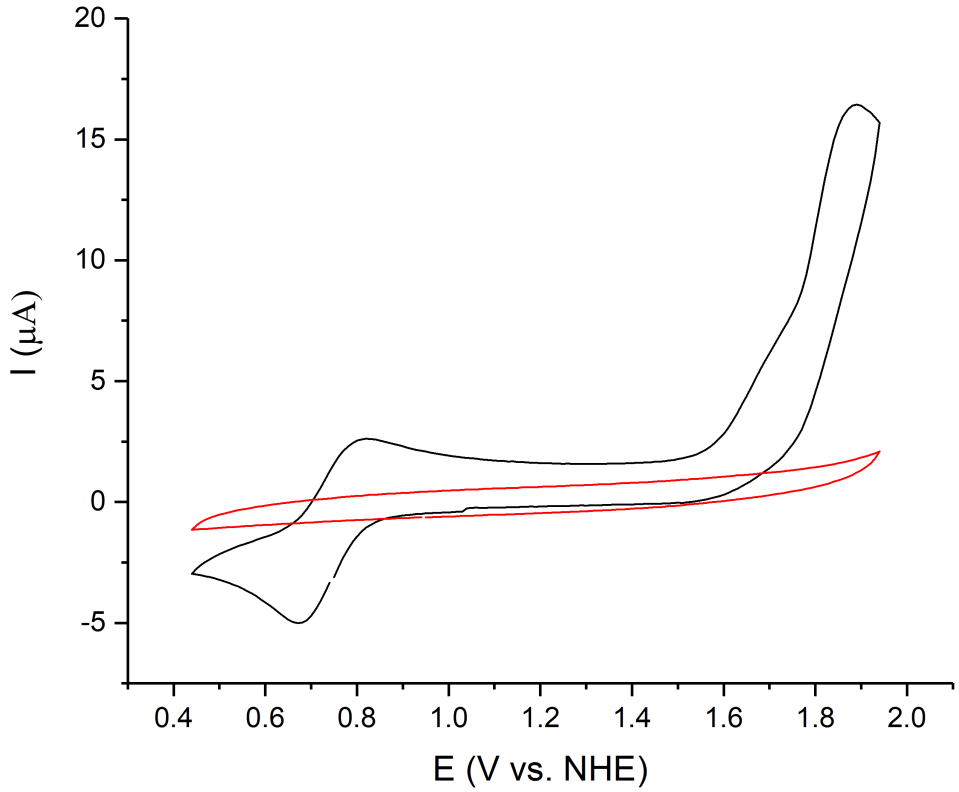

Figure S9. CV of 1 mM **3** in pure TFE with a scan rate of 10 mV s^{-1}. Two glassy carbon electrodes were used as working and counter electrode and a $Ag/AgNO_3$ electrode was used as a reference electrode. The red curve is the CV of the pure solvent.

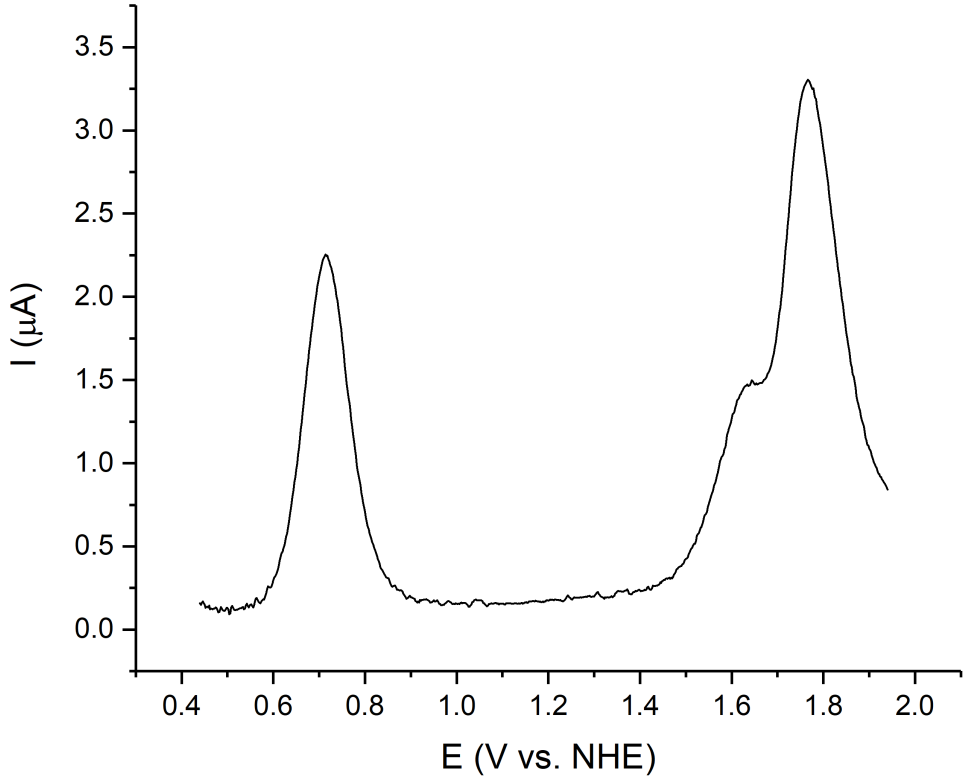

Figure S10. DPV of **3** in pure TFE. Two glassy carbon electrodes were used as working and counter electrode and a $Ag/AgNO_3$ electrode was used as a reference electrode. The scan rate was 0.002 mV s^{-1}, the pulse height was 50 mV, the pulse time was 0.3 s and the potential step was 2 mV.

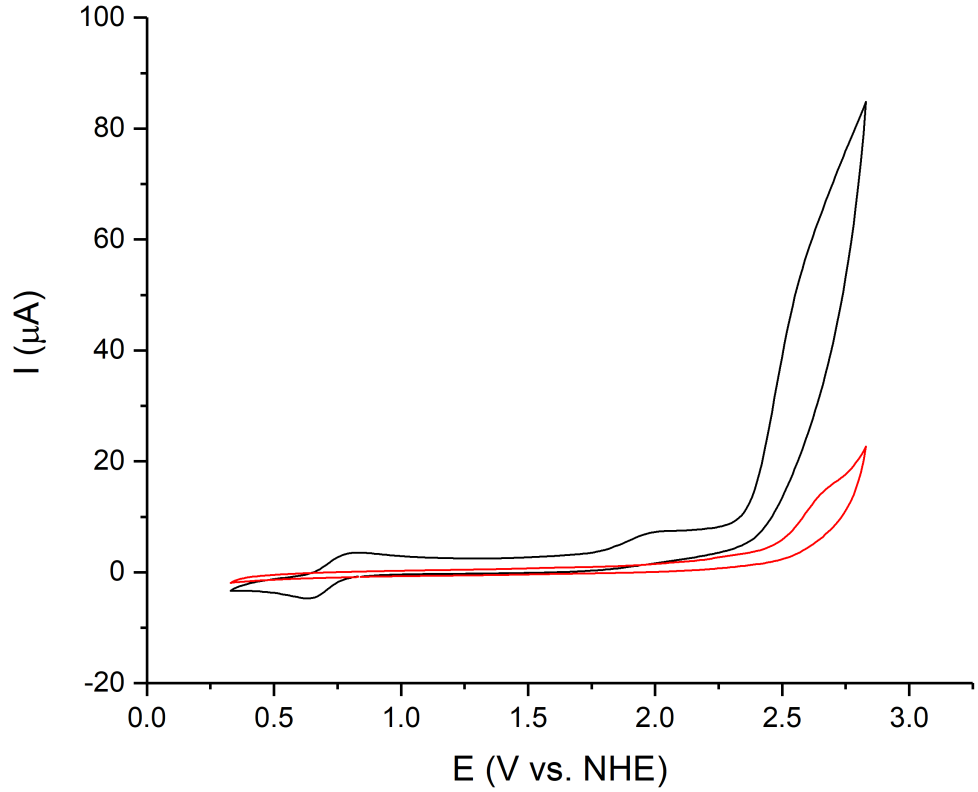

Figure S11. CV of 1 mM **2** in pure TFE with a scan rate of 100 mV s^{-1}. Two glassy carbon electrodes were used as working and counter electrode and an $Ag/AgNO_3$ electrode was used as a reference electrode. The red curve is the CV of the pure solvent.

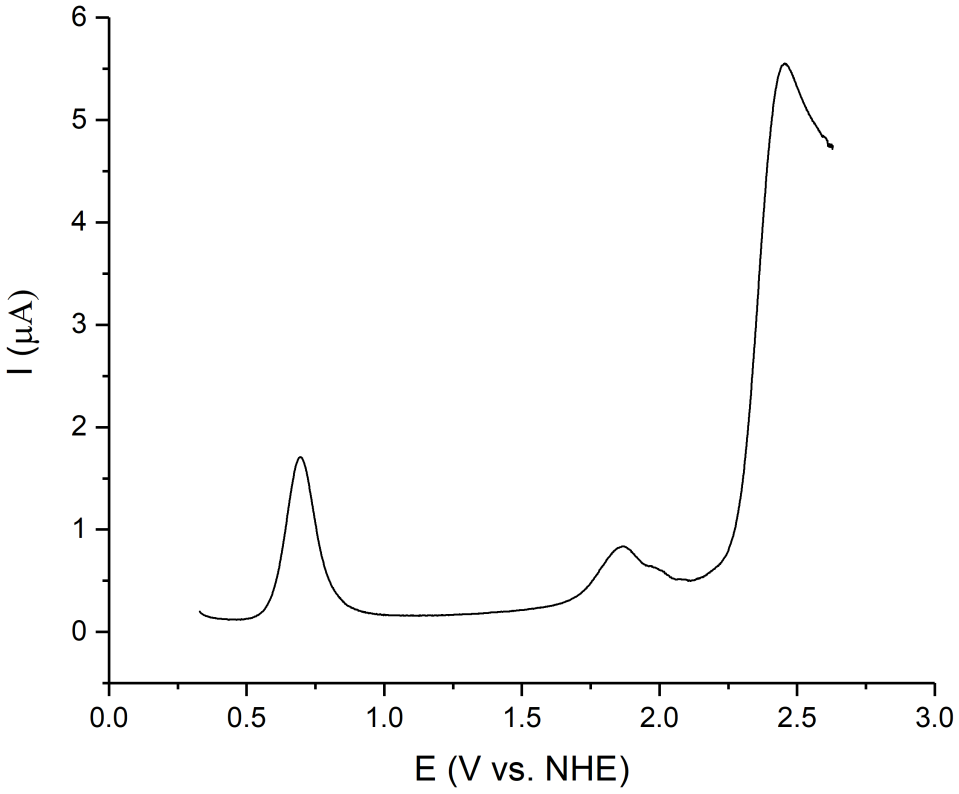

Figure S12. DPV of **2** in pure TFE. Two glassy carbon electrodes were used as working and counter electrode and an $Ag/AgNO_3$ electrode was used as a reference electrode. The scan rate was 0.002 mV s^{-1}, the pulse height was 50 mV, the pulse time was 0.3 s and the potential step was 2 mV.

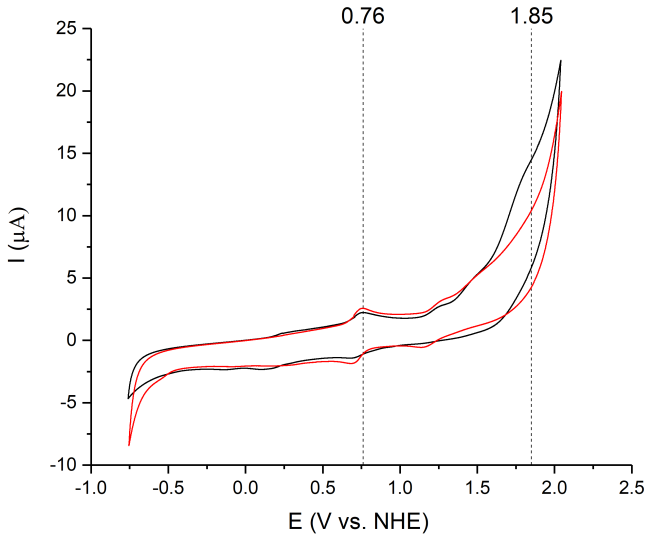

Figure S13. CV of **2** and **3** in 2:1, TFE/pH 1_{aq} at a scan rate of 10 mV s^{-1}. The vertical lines represent the potentials at which the values for $i_{p,anodic}$ (0.76 V) and $i_{cat,anodic}$ (1.85 V) were taken. Two glassy carbon electrodes were used as working and counter electrode and an Ag/AgCl electrode was used as reference electrode.

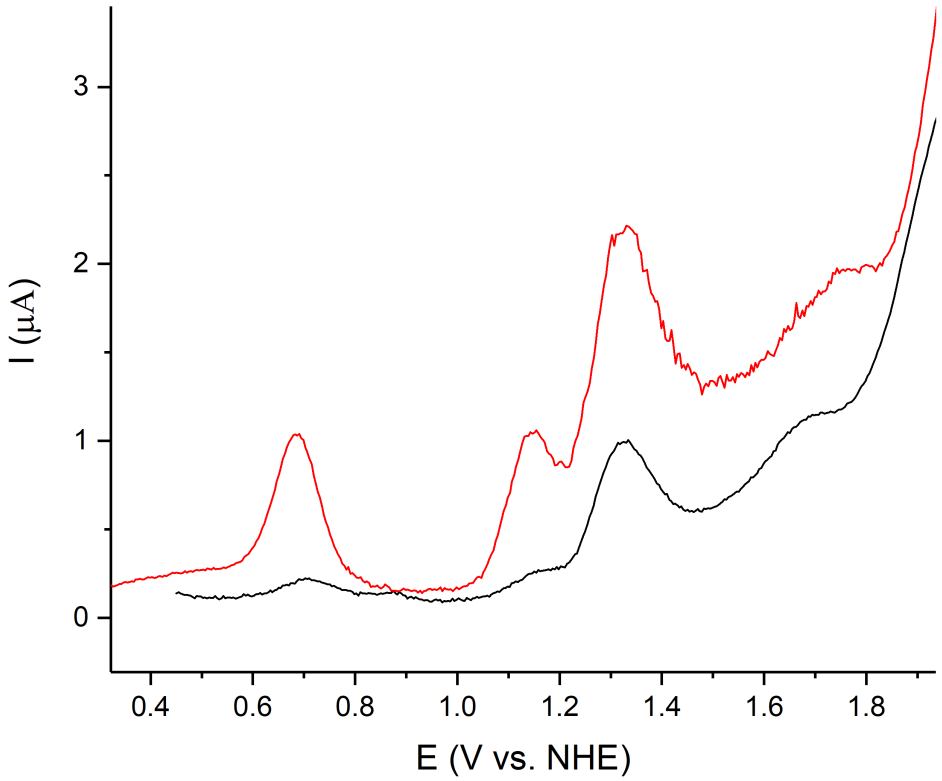

Figure S14. DPV measurement for **2** (red) and **3** (black) in the 1:2 TFE/pH 1_{aq} mixture, under the optimized conditions for **2** The measurement was recorded with a pulse amplitude of 50 mV, a pulse width of 2.5 s, a step width of 5 s, a step height of 4 mV, a sampling time of 500 ms for **2**, and of 25 ms for **3**. The low solubility of **3** under these conditions prevented further analysis.

Table S1. Reaction energetics (kcal mol^{-1}) including reaction barriers for catalysts **1**, **2**, and **3**, computed at TPSSh-D3(BJ)/def2-QZVPP(d)/ε=78 level values within parentheses, and spin populations for Ru-O.

Catalyst/State	Dimer	Transition state	Peroxy	Dioxygen
1/*S*=0				
Δ*H*(*T*=298K)	-2.1	+5.7	-9.7	+2.7
Δ*G*(*T*=298K)	+11.9	+21.5	+4.8	+16.6
E(disp)	-19.0	-21.1	-19.0	-17.5
Ru-O spin density	+0.48 / +0.55	+0.21 / +0.37	0 / 0	+0.62 / -0.58
Ru'-O' spin density	-0.48 / -0.55	-0.21 / -0.37	0 / 0	+0.36 / -0.54
1/*S*=1				
Δ*H*(*T*=298K)	-2.3	+17.2	+10.7	+3.9
Δ*G*(*T*=298K)	+11.6	+32.0	+27.8	+18.5
E(disp)	-18.8	-20.1	-17.9	-17.3
Ru-O spin density	+0.48 / +0.55	+1.19 / +0.20	+0.02 / +0.04	+0.70 / +0.68
Ru'-O' spin density	+0.48 / +0.55	+0.11 / +0.34	+1.41 / +0.17	+0.08 / +0.41
2/*S*=0				
Δ*H*(*T*=298K)	-10.5	-8.6	-18.8	-8.5
Δ*G*(*T*=298K)	+6.0	+9.5	-1.3	+8.6
E(disp)	-33.9	-35.3	-36.7	-34.2
Ru-O spin density	+0.47 / +0.57	+0.18 / +0.34	0 / 0	+0.72 / -0.56
Ru'-O' spin density	-0.47 / -0.57	-0.18 / -0.34	0 / 0	+0.13 / -0.40
2/*S*=1				
Δ*H*(*T*=298K)	-10.5	+12.8	-0.4	-7.5
Δ*G*(*T*=298K)	+6.0	+29.6	+16.2	+9.3
E(disp)	-34.2	-36.2	-36.2	-33.3
Ru-O spin density	+0.47 / +0.56	+1.15 / +0.20	+0.02 / +0.04	+0.73 / +0.72
Ru'-O' spin density	-0.47 / -0.56	+0.20 / +0.29	+1.45 / +0.13	+0.03 / +0.39

Table S1. (contd.) Reaction energetics (kcal mol^{-1}) including reaction barriers for catalysts **1**, **2**, and **3**, computed at TPSSh-D3(BJ)/def2-QZVPP(d)/ε=78 level values within parentheses, and spin populations for Ru-O.

3/*S*=0				
Δ*H*(*T*=298K)	-19.6	-15.7	-26.4	-12.0
Δ*G*(*T*=298K)	-2.7	+3.3	-8.2	+5.0
E(disp)	-43.3	-46.8	-47.7	-45.5
Ru-O spin density	+0.45 / +0.55	+0.17 / +0.34	0 / 0	+0.62 / -0.70
Ru'-O' spin density	-0.45 / -0.55	-0.17 / -0.34	0 / 0	+0.62 / -0.70
3/*S*=1				
Δ*H*(*T*=298K)	-19.5	+7.4	-7.8	-11.5
Δ*G*(*T*=298K)	-2.5	+25.1	+9.4	+6.3
E(disp)	-42.7	-47.9	-47.5	-45.8
Ru-O spin density	+0.46 / +0.57	+1.15 / +0.18	+0.02 / +0.03	+0.67 / +0.69
Ru'-O' spin density	-0.46 / -0.57	+0.20 / +0.26	+1.40 / +0.12	+0.05 / +0.47

Transition state frequencies (cm^{-1})	***S*=0**	***S*=1**
1	234*i*	537*i*
2	192*i*	450*i*
3	214*i*	452*i*

Table S2. Comparison of RPA and DFT reaction energetics for catalysts **1**, **2**, and **3**, computed at TPSSh-D3(BJ)/def2-QZVPP(d)/ε=78 and RPA/def2-[T,Q]ZVPP(D) levels.

Catalyst/State		**Dimer**		**Transition state**		**Peroxy**		**Dioxygen**	
		DFT	RPA	DFT	RPA	DFT	RPA	DFT	RPA
1/*S*=0	Δ*H*(*T*=298K)	-2.1	-2.2	+5.7	+6.3	-9.7	-9.4	+2.7	+2.8
	Δ*G*(*T*=298K)	+11.9	+11.8	+21.5	+22.1	+4.8	+5.1	+16.6	+16.7
2/*S*=0	Δ*H*(*T*=298K)	-10.5	-12.4	-8.6	-5.7	-18.8	-17.7	-8.5	-6.8
	Δ*G*(*T*=298K)	+6.0	+4.1	+9.5	+12.4	-1.3	-0.2	+8.6	+10.3
3/*S*=0	Δ*H*(*T*=298K)	-19.6	-20.1	-15.7	-12.6	-26.4	-24.6	-12.0	-9.5
	Δ*G*(*T*=298K)	-2.7	-3.2	+3.3	+6.4	-8.2	-6.4	+5.0	+7.5

Table S3. Energy decomposition analysis (EDA) of the open-shell singlet pre-complex dimer (top) and transition states (below) of catalysts **1**, **2**, and **3** in kcal mol^{-1} (energies relative to catalyst **2** in parentheses).

Interaction (dimer)	**1**		**2**	**3**	
Electrostatics	+14.0	*(+14.4)*	-0.5	+3.3	*(+3.8)*
Pauli repulsion	+32.7	*(-31.8)*	+64.5	+70.4	*(+5.9)*
Polarization	-8.9	*(+8.8)*	-17.7	-15.9	*(+1.8)*
Electron correlation	-10.8	*(+8.4)*	-19.2	-23.0	*(-3.8)*
Dispersion	-19.0	*(+14.9)*	-33.9	-43.2	*(-9.3)*
Solvation	-15.0	*(-4.1)*	-10.9	-15.0	*(-4.1)*
Geometric strain	+3.3	*(-2.2)*	+5.5	+2.4	*(-0.0)*
Entropy	+15.8	*(-2.4)*	+18.2	+8.3	*(+0.1)*
Total	**+12.0**	***(+6.0)***	**+6.0**	**-2.7**	***(-8.7)***

Interaction (TS)	**1**		**2**	**3**	
Electrostatics	-15.7	*(-5.0)*	-10.6	-16.7	*(-6.1)*
Pauli repulsion	+98.9	*(-15.8)*	+114.6	+133.0	*(+18.3)*
Polarization	-37.8	*(+2.1)*	-39.9	-43.3	*(-3.5)*
Electron correlation	-18.7	*(+7.3)*	-26.0	-31.9	*(-6.0)*
Dispersion	-21.1	*(+14.2)*	-35.2	-46.7	*(-11.5)*
Solvation	-5.1	*(+11.4)*	-16.4	-14.6	*(+1.9)*
Geometric strain	+5.0	*(+1.0)*	+4.0	+3.9	*(-0.0)*
Entropy	+15.9	*(-3.1)*	+19.0	+19.6	*(+0.6)*
Total	**+21.5**	***(+12.0)***	**+9.5**	**+3.3**	***(-6.2)***

Table S4. Selected bond lengths (Å) and angles (°) for the Ru(II)-Bda complexes, obtained from crystallographic data.

Bond/Angle	**1**[a)]	**2**	**3**
Ru – O1	2.216(7)	2.172(3)	2.177(4)
Ru – O3	2.172(7)	2.165(3)	2.195(4)
Ru – N_{eq}	1.914(7)/1.950(7)	1.929(4)/1.928(3)	1.935(5)/1.931(6)
Ru – N_{ax}	2.084(6)/2.070(6)	2.082(4)/2.078(4)	2.077(5)/2.061(5)
O1 – Ru–O2	123.0(2)	121.4(1)	121.6(2)
$Ax(1)_{plane}$ – $Ax(2)_{plane}$	22.3(3)	14.25	28.47
π-π distances	n/a	3.51	3.37 – 3.48

[a)] From ref [21].

Table S5. Peak current values of the $Ru^{III/II}$ couple at 760 mV, and of $i_{cat}/i_{p,anodic}$ at E^{ox} = 1.85 V, from the CV data of three different samples of **2** and **3**. From the above data, the ratio of i_{cat}/i_p for **3**:**2** was calculated as 1.69, which yields a ratio of $k_{obs,3}$: $k_{obs,2}$ = 2.88. This value is only valid under the specific CV conditions used (10 mV s^{-1}, 2:1 TFE/pH 1_{aq}), and may differ at other scan rates. We have not taken into account a concentration dependence in Eqn. 1, which is included in FOWA in cases where dimerization is rate-limiting.

Compound	$i_{p,anodic}$ [µA]	$i_{cat,anodic}/i_{p,anodic}$	Measurement
	2.590	4.122	1
2	2.049	4.043	2
	1.985	4.135	3
	1.858	6.659	1
3	1.512	6.867	2
	1.493	7.030	3

Table S6. Crystallographic data for **2 · 2 $CHCl_3$**.

Chemical formula	$C_{32}H_{22}Cl_6N_4O_4Ru$	
Formula weight	840.31	
Temperature	100(2) K	
Wavelength	0.71073 Å	
Crystal size	0.058 x 0.139 x 0.172 mm	
Crystal system	monoclinic	
Space group	$P\ 2_1/n$	
Unit cell dimensions	a = 8.9053(5) Å	α = 90°
	b = 14.6973(8) Å	β = 99.0280(10)°
	c = 27.8975(14) Å	γ = 90°
Volume	3606.1(3) $Å^3$	
Z	4	
Density (calculated)	1.548 g/cm^3	
Absorption coefficient	0.920 mm^{-1}	
F(000)	1680	
Theta range for data collection	2.32 to 25.03°	
Index ranges	-10<=h<=10, -17<=k<=17, -33<=l<=33	
Reflections collected	74764	
Independent reflections	6391 [R(int) = 0.1270]	
Max. and min. transmission	0.9490 and 0.8580	
Refinement method	Full-matrix least-squares on F^2	
Refinement program	SHELXL-2018/3 (Sheldrick, 2018)	
Function minimized	$\Sigma\ w(F_o^2 - F_c^2)^2$	
Data / restraints / parameters	6391 / 0 / 425	
Goodness-of-fit on F^2	1.056	
Δ/σ_{max}	0.001	
Final R indices	4808 data; I>2σ(I)	R1 = 0.0541, wR2 = 0.0907
	all data	R1 = 0.0841, wR2 = 0.989
Weighting scheme	$w=1/[\sigma^2(F_o^2)+(0.1055P)^2+71.3880P]$ where $P=(F_o^2+2F_c^2)/3$	
Largest diff. peak and hole	0.618 and -0.712 $eÅ^{-3}$	
R.M.S. deviation from mean	0.105 $eÅ^{-3}$	

Table S7. Crystallographic data for **3·2DCM·H_2O**

Chemical formula	$C_{40}H30Cl_4N_4O_5Ru$	
Formula weight	889.55	
Temperature	100(2) K	
Wavelength	0.71073 Å	
Crystal size	0.256 x 0.130 x 0.050 mm	
Crystal system	monoclinic	
Space group	*P* $2_1/c$	
Unit cell dimensions	*a* = 12.780(4) Å	α = 90°
	b = 14.131(5) Å	β = 101.067(10)°
	c = 24.436(8) Å	γ = 90°
Volume	4331.(2) Å3	
Z	4	
Density (calculated)	1.364 g/cm^3	
Absorption coefficient	0.653 mm^{-1}	
F(000)	1800	
Theta range for data collection	2.21 to 25.37°	
Index ranges	-15<=h<=15, -16<=k<=17, -29<=l<=25	
Reflections collected	46578	
Independent reflections	7912 [R(int) = 0.0927]	
Refinement method	Full-matrix least-squares on F2	
Refinement program	SHELXL-2018/3 (Sheldrick, 2018)	
Function minimized	Σ w(Fo2 - Fc2)2	
Data / restraints / parameters	7912 / 2 / 491	
Goodness-of-fit on F^2	1.116	
Δ/σ_{max}	0.001	
Final R indices	6258 data; I>2σ(I)	R1 = 0.0757, wR2 = 0.1662
	all data	R1 = 0.0981, wR2 = 0.1758
Weighting scheme	w=1/[σ2(Fo2)+(0.0368P)2+44.8992P] where P=(Fo2+2Fc2)/3	
Largest diff. peak and hole	1.081 and -1.136 eÅ^{-3}	
R.M.S. deviation from mean	0.132 eÅ^{-3}	

SI References

(1) V. N. Staroverov, G.E Scuseria, J. Tao, J. P. Perdew, Comparative Assessment of a New Nonempirical Density Functional: Molecules and Hydrogen-Bonded Complexes. *J. Chem. Phys.* **2003**, *119*, 12129–12137.

(2) S. Grimme, J. Antony, S. Ehrlich,H. Krieg, A Consistent and Accurate Ab Initio Parametrization of Density Functional Dispersion Correction (DFT-D) for the 94 Elements H-Pu. *J. Chem. Phys.* **2010**, *132*, 154104.

(3) A. D. Becke, E. R. Johnson, A Density-Functional Model of the Dispersion Interaction. *J. Chem. Phys.* **2005**, *123*, 154101.

(4) S. Grimme, S. Ehrlich, L. Goerigk, Effect of the Damping Function in Dispersion Corrected Density Functional Theory. *J. Comput. Chem.* **2011**, *32*, 1456–1465.

(5) F. Weigend, R. Ahlrichs, Balanced Basis Sets of Split Valence, Triple Zeta Valence and Quadruple Zeta Valence Quality for H to Rn: Design and Assessment of Accuracy. *Phys. Chem. Chem. Phys.* **2005**, *7*, 3297–3305.

(6) D. Rappoport, F. Furche, Property-Optimized Gaussian Basis Sets for Molecular Response Calculations. *J. Chem. Phys.* **2010**, *133*, 134105.

(7) A. Klamt, G. Schüürmann, COSMO: A New Approach to Dielectric Screening in Solvents with Explicit Expressions for the Screening Energy and Its Gradient. *J. Chem. Soc. Perkin Trans.* 2 **1993**, No. 5, 799–805.

(8) P. Plessow, Reaction Path Optimization without NEB Springs or Interpolation Algorithms. *J. Chem. Theory Comput.* **2013**, *9*, 1305–1310.

(9) E. Weinan, W. Ren, E. Vanden-Eijnden, String Method for the Study of Rare Events. Phys. Rev. B 2002, *66*, 052301.

(10) F. Furche, Molecular Tests of the Random Phase Approximation to the Exchange-Correlation Energy Functional. *Phys. Rev. B* **2001**, *64*, 195120.

(11) H. Eshuis, J. E. Bates, F. Furche, Electron Correlation Methods Based on the Random Phase Approximation. *Theor. Chem. Acc.* **2012**, *131*, 1084.

(12) G. P. Chen, V. K. Voora, M. M. Agee, S. G. Balasubramani, F. Furche, Random-Phase Approximation Methods. *Annu. Rev. Phys. Chem.* **2017**, *68*, 421–445.

(13) H. Eshuis, F. Furche, A Parameter-Free Density Functional That Works for Noncovalent Interactions. *J. Phys. Chem. Lett.* **2011**, *2*, 983–989.

(14) A. Halkier, R. Helgaker, P. Jørgensen, W. Klopper, H. Koch, J. Olsen, A. K. Wilson, Basis-Set Convergence in Correlated Calculations on Ne, N_2, and H_2O. *Chem. Phys. Lett.* **1998**, *286*, 243–252.

(15) E. R. Johnson, S. Keinan, P. Mori-Sánchez, J. Contreras-García, A. J. Cohen, A. W.Yang, Revealing Noncovalent Interactions. *J. Am. Chem. Soc.* **2010**, *132*, 6498–6506.

(16) J. Contreras-García, E. R. Johnson, E. S. Keinan, R. Chaudret, J.-P.Piquemal, D. N. Beratan, D. W. Yang, NCIPLOT: A Program for Plotting Noncovalent Interaction Regions. *J. Chem. Theory Comput.* **2011**, *7*, 625–632.

(17) W. Humphrey, A. Dalke, K. Schulten, VMD: Visual Molecular Dynamics. J. Mol. Graph. 1996, *14*, 33–38.

(18) P. Su, H. Li, *J. Chem. Phys.* **2009**, *131*, 014102.

(19) R. Ahlrichs, M.Bär, M. Häser, H. Horn, C. Kölmel,Electronic Structure Calculations on Workstation Computers: The Program System TURBOMOLE. *Chem. Phys. Lett.* **1989**, *162*, 165–169.

(20) Turbomole V7.1-7.3, 2016-2018, a Development of University of Karlsruhe and Forschungszentrum Karlsruhe GmbH, 1989-2007, TURBOMOLE GmbH, since 2007; Available from http://www.turbomole.com.

(21) E. Dulière, M. Devillers, J. Marchand-Brynaert, Novel Phosphinite-Ruthenium(II) Complexes Covalently Bound on Silica: Synthesis, Characterization, and Catalytic Behavior versus Oxidation Reactions of Alcohols into Aldehydes. *Organometallics* **2003**, 22, 804–811.

(22) L. Duan, F. Bozoglian, S. Mandal, B. Stewart, T. Privalov, A. Llobet, L. Sun, A Molecular Ruthenium Catalyst with Water-Oxidation Activity Comparable to That of Photosystem II. *Nat. Chem.* **2012**, *4*, 418–423.

(23) A. P. Krapcho, T. P. Gilmor, General Synthetic Route to Benz[g]Isoquinolines (2-Azaanthracenes). *J. Heterocycl. Chem.* **1998**, *35*, 669–674.

(24) *APEX Suite of Crystallographic Software*, APEX 3, Version 2015-5.2. Bruker AXS Inc.: Madison, Wisconsin, USA 2015.

(25) *SAINT*, Version 8.34A. Bruker AXS Inc.: Madison, Wisconsin, USA 2014; *SAINT*, Version 8.38A. Bruker AXS Inc.: Madison, Wisconsin, USA 2015.

(26) *SADABS*, Version 2014/5. Bruker AXS Inc.: Madison, Wisconsin, USA 2014; L. Krause, R. Herbst-Irmer, G. M. Sheldrick, G. D. Stalke, Comparison of Silver and Molybdenum Microfocus X-Ray Sources for Single-Crystal Structure Determination. *J. Appl. Crystallogr.* **2015**, *48*, 3–10.

(27) G. M. Sheldrick, SHELXT - Integrated Space-Group and Crystal-Structure Determination. *Acta Crystallogr. Sect. A Found. Crystallogr.* **2015**, *71*, 3–8.

(28) G. M. Sheldrick, Crystal Structure Refinement with SHELXL. *Acta Crystallogr. Sect. C Struct. Chem.* **2015**, *71*, 3–8.

(29) C. B. Hübschle, G. M. Sheldrick, B. Dittrich, B. ShelXle: A Qt Graphical User Interface for SHELXL. *J. Appl. Crystallogr.* **2011**, *44*, 1281–1284.

(30) C. F. Macrae, I. J. Bruno, J. A. Chisholm, P. R. Edgington, P. McCabe, E. Pidcock, L. Rodriguez-Monge, R. Taylor, J. Van De Streek, P. A. Wood, Mercury CSD 2.0 - New Features for the Visualization and Investigation of Crystal Structures. *J. Appl. Crystallogr.* **2008**, *41*, 466–470.

(31) A. L. Spek, Structure Validation in Chemical Crystallography. *Acta Crystallogr. Sect. D Biol. Crystallogr.* **2009**, *65*, 148–155.

(32) E. S. Rountree, B. D. McCarthy, T. T. Eisenhart, J. L. Dempsey, Evaluation of Homogeneous Electrocatalysts by Cyclic Voltammetry. *Inorg. Chem.* **2014**, *53*, 9983–10002.

(33) R. Matheu, M. Z. Ertem,C. Gimbert-Suriñach, X. Sala, A. Llobet, Seven Coordinated Molecular Ruthenium‐Water Oxidation Catalysts: A Coordination Chemistry Journey. *Chem. Rev.* **2019**, *119*, 3453‐3471.